HHS Public Access

Author manuscript

Biochem Biophys Res Commun. Author manuscript; available in PMC 2019 September 26.

Published in final edited form as:

Biochem Biophys Res Commun. 2018 September 26; 504(1): 89–95. doi:10.1016/j.bbrc.2018.08.135.

Molecular mechanism for the inhibition of DXO by adenosine 3', 5'-bisphosphate

Ji-Sook Yun[#a], **Je-Hyun Yoon**[#b], **Young Jun Choi**[a], **Young Jin Son**[c,2], **Sung Hwan Kim**[c,3], **Liang Tong**[d,*], and **Jeong Ho Chang**[a,d,*]

[a]Department of Biology Education, Kyungpook National University, Daegu 41566, South Korea

[b]Department of Biochemistry and Molecular Biology, Medical University of South Carolina, Charleston, SC 29425, USA

[c]New Drug Development Center, Daegu-Gyungpook Medical Innovation Foundation, Daegu 41061, South Korea.

[d]Department of Biological Sciences, Columbia University, New York, NY 10027, USA

[#] These authors contributed equally to this work.

Abstract

The decapping exoribonuclease DXO functions in pre-mRNA capping quality control, and shows multiple biochemical activities such as decapping, deNADding, pyrophosphohydrolase, and 5'−3' exoribonuclease activities. Previous studies revealed the molecular mechanisms of DXO based on the structures in complexes with a product, substrate mimic, cap analogue, and 3'-NADP$^+$. Despite several reports on the substrate- specific reaction mechanism, the inhibitory mechanism of DXO remains elusive. Here, we demonstrate that adenosine 3', 5'-bisphosphate (pAp), a known inhibitor of the 5'−3' exoribonuclease Xrn1, inhibits the nuclease activity of DXO based on the results of structural and biochemical experiments. We determined the crystal structure of the DXO-pAp-Mg^{2+} complex at 1.8 Å resolution. In comparison with the DXO-RNA product complex, the position of pAp is well superimposed with the first nucleotide of the product RNA in the vicinity of two magnesium ions. Furthermore, biochemical assays showed that the inhibition by pAp is comparable between Xrn1 and DXO. Collectively, these structural and biochemical studies reveal that pAp inhibits the activities of DXO by occupying the active site to act as a competitive inhibitor.

[*]Corresponding authors: Liang Tong, Phone: +1-212-854-5203, Fax: +1-212-865-8246, ltong@columbia.edu, Jeong Ho Chang, Phone: +82-53-950-5913, Fax: +82-53-950-6809, jhcbio@knu.ac.kr.

[2]Present address: Department of New Drug Discovery, Samhyun Inc., Daegu 41061, South Korea

[3]Present address: R&D center, Polus Inc., 32 Songdogwahak-ro, Yeonsu-gu, Incheon 21984, South Korea

Conflict of interest

The authors have no conflict of interest to declare.

Keywords

5’−3’ exoribonuclease; DXO; adenosine 3’,5’-bisphosphate; crystal; nuclease inhibitor

1. Introduction

In eukaryotes, expression of a particular gene is tightly regulated in a coordinated manner via several interconnected processes, including mRNA synthesis and processing in the nucleus, mRNA export via nuclear pore complex, mRNA translation, and eventually mRNA degradation [1, 2]. In these processes, the degradative events of mRNA are important determinants of gene expression, which are driven by diverse integral components of RNA metabolism [3]. Thus, the mRNA degradative pathways comprise various sets of enzymes such as Dcp1/2, Xrn1, exosomes, and Ccr4-Caf1 with important biochemical activities, including decapping, exonucleolysis, and deadenylation [4–6]. The mechanisms of both the 5’−3’ and 3’−5’ exoribonuclease reaction are well studied based on three-dimensional structures [7–9]

Although the mRNA capping process was previously thought to be devoid of any quality control mechanism, 5’-end capping surveillance mechanisms in yeast and mammalian cells are now known to help discriminate incomplete capped mRNAs and then degrade them in a two-step process involving the decapping and 5’−3’ exoribonuclease activities of DXO [10–12]. Therefore, these surveillance pathways involve the function of DXO in mRNA quality control for ensuring RNA fidelity. DXO was originally designated as Rai1/Ydr370c and Dom3Z in fungal species and mammals, respectively [13]. We previously determined the detailed distinct substrate specificity and biochemical activities among Rai1, Ydr370c (Dxo1), and DXO proteins in 5’−3’ exoribonuclease and decapping activities based on their crystal structures in complex with their substrate mimic or product [10, 12, 14].

Recently, 5’ end nicotinamide dinucleotide (NAD^+)-capped mRNAs were found in human cells rather than the m7G cap, which could promote decay via a DXO-mediated deNADding mechanism [15, 16]. The 5’ end NAD^+ was initially found in bacteria and can initiate selective mRNA decay by NudC, which hydrolyzes the NAD^+ to generate nicotinamide mononucleotide (NMN) and 5’ monophosphorylated RNA, which could be degraded by 5’−3’ exoribonucleases [17, 18]. As similar to NudC, DXO can remove the NAD^+-capped RNA by both deNADding and degrade RNA using its 5’−3’ exoribonuclease activity in human cells [15]. The crystal structure of DXO in complex with 3’ phosphate NAD^+ revealed the deNADding mechanism in which the scissile phosphate position is shared with that of the substrate mimic RNA pU(S)6 [15].

Adenosine 3’, 5’ bisphosphate (pAp) was initially reported as an inhibitor of the 5’−3’ exoribonuclease activity of Xrn1 and Rati [19]. In Saccharomyces cerevisiae, pAp is produced from 3’-phosphoadenosine 5’-phosphosulfate (pApS) by Met16p, and is then converted to AMP and inorganic phosphate by Hal2 during sulfate assimilation [20]. Lithium inhibits Hal2 or Met22 to induce pAp accumulation, resulting in toxic effects. An elevated level of pAp was shown to reduce the activity of Xrni or Rati as well as Oligoribonuclease (Orn) in Escherichia *coli* and small fragment nuclease (Sfn) in humans

that inhibits RNA metabolism such as mRNA turnover and transcription [21]. Inhibitory aptamers of DXO containing a 5'-GGATCCC-3' motif were recently reported using a microplate-based microcolumn device (MEDUSA), which is an improved version of the aptamer screening method, and five candidates were evaluated by an *in vitro* 5'−3' exoribonuclease activity assay [22].

To understand the inhibitory mechanism of DXO, in the present study we determined the crystal structure of DXO in complex with pAp and Mg^{2+} at 1.8 Å resolution and we examined the effects of pAp on the 5'−3' exoribonuclease activity of DXO, using Xrn1 for comparison. In addition, we compared the nuclease activity and pAp-binding affinity between DXO and Xrn1.

2. Materials and Methods

2.1. Protein expression, purification, and crystallization

Protein expression, purification, and crystallization of mammalian DXO were carried out as described previously [10, 23]. In brief, E234A mutant protein and the wild-type enzyme were purified by Ni-NTA and gel filtration chromatography using the same protocol. Free enzyme crystals of DXO were obtained with the sitting-drop vapor diffusion method at 20°C, using a reservoir solution containing 20% (w/v) PEG 3350. The pAp-Mg^{2+} complex was obtained by soaking the free enzyme crystals with 100 mM pAp (Sigma A5763) and 10 mM $MgCl^2$ for 60 min in the presence of 15% ethylene glycol. Crystals were flash-frozen in liquid nitrogen for diffraction analysis and data collection at 100 K.

2.2. Data collection and structure determination

X-ray diffraction data were collected at the National Synchrotron Light Source (NSLS) beamline X29A. The diffraction images were processed and scaled with the HKL package [24]. The crystals belong to space group $P2_1$, with the following cell parameters: a = 50.0 Å, b = 87.7 Å, c = 53.9 Å, and β = 112.2°. There is one molecule of DXO in the crystallographic asymmetric unit. Structure refinement was carried out with the CNS program [25]. The atomic model was built with the program Coot [26]. The crystallographic information is summarized in Table 1.

2.3. Exonuclease assays with fluorescently labeled RNA

The 3'-FAM-labeled 30-mer RNA with 5'-end monophosphate [27] and the equivalent single-stranded DNA oligos were purchased from Integrated DNA Technologies (IDT). Exonuclease assays were performed at 37°C for 30 min with reaction mixtures containing 30 mM Tris (pH 8.0), 50 mM NH_4Cl, 2 mM $MgCl_2$, 0.5 mM dithiothreitol, 25 μg/ml bovine serum albumin, 2 μM 3'-FAM-labeled oligo, 0.1—1 μM DXO, and 0.01—0.1 μM Xrn1. The products were fractionated by 5% denaturing polyacrylamide gel electrophoresis and visualized on an ultraviolet illuminator. Assays were repeated at least three times to ensure reproducibility.

2.4. Surface plasmon resonance analysis

The molecular interactions were determined by surface plasmon resonance (SPR) binding analysis as described previously [28, 29]. Real-time protein inhibitor interactions were examined on a BIAcore instrument (BIAcore T200). DXO and Xrn1 were immobilized on a CM5 sensor chip using the amine-coupling method (GE Healthcare Life Sciences) according to the manufacturer's instructions. In brief, native DXO (25 μg/ml) or Xrn1 (25 μg/ml) was immobilized on a single N-hydroxysuccinimide-activated flow cell, and a reference flow cell was prepared by activating the surface. Remaining activated groups on each flow cell were blocked by ethanolamine HCl. The chip was then washed with 0.1 M NaOH to remove any non-covalently bound proteins. Finally, the system was primed with the running buffer comprising 50 mM phosphate buffer, pH 7.8, 150 mM NaCl, 5 mM $MgCl_2$, 0.05% P20, and 0.1 mg/ml bovine serum albumin. A range of concentrations (0.5, 1, 2, 4, 8 mM) of pAp and GTP were prepared in the running buffer and injected at a 30 μl/min flow rate. The sensorgram data were processed by subtracting the signals from the reference cell and a blank injection of the running buffer.

3. Results

3.1. pAp inhibits the 5 '−3 ' exoribonuclease activity of DXO

On the basis of the 5'−3' exoribonuclease activity of DXO, we compared the nuclease activity between DXO and Xrn1. The processive 5'−3' exoribonuclease Xrn1 showed almost 20-fold higher nuclease activity than that of the distributive 5'−3' exoribonuclease DXO (Fig. 1A). We next assessed whether pAp can inhibit the nuclease activity of DXO. The 5'−3' exoribonuclease activity of DXO at 0.5 pM was inhibited by pAp starting from 0.5 mM, and 20 mM of pAp completely blocked the activity (Fig. 1B). To compare the potency of pAp inhibition between DXO and Xrn1, we performed a nuclease activity assay of Xrn1 in the presence of pAp. The activity of Xrn1 at 0.02 μM was reduced by pAp at concentrations greater than 0.5 mM and was completely inhibited by 10 mM pAp (Fig. 1B). The activity of DXO was completely inhibited by an approximately 40,000-fold molar ratio of pAp, and loss of Xrn1 activity was detected with an approximately 500,000-fold molar ratio of pAp. Based on these results, the inhibitory potency of pAp toward the nuclease activity seemed to be slightly higher for DXO than for Xrn1. However, direct comparison of pAp-mediated inhibition may be controversial because more DXO could facilitate the formation of pAp complex in the assay, thereby requiring less pAp for complete inhibition. Moreover, in the presence of pAp, the DXO products got smaller (Fig. 1B). On the other hand, Xrn1 still showed no intermediate. Furthermore, DXO and Xrn1 are distributive and processive nucleases, respectively.

3.2. Comparison of pAp binding affinity on DXO and Xrn1

To address whether the binding affinity of pAp is responsible for the difference in the inhibitory effect on DXO and Xrn1, we performed a surface plasmon resonance experiment with both DXO and Xrn1. Varied concentrations of pAp, ranging from 0.5 mM to 8 mM, were treated to the immobilized DXO and Xrn1 protein on the chip. Both DXO and Xrn1 showed clear concentration-dependent interactions (Fig. 1C, D). The dissociation constants of pAp for DXO and Xrn1 were likely 20 ~ 30 mM range, but could not be determined

accurately because of low affinity. To test whether these experiments are due to artifacts, we obtained the sensorgrams of GTP binding to DXO and Xrn1 as negative controls, and did not detect any signals generated from 8 mM GTP binding on both proteins (data not shown).

3.3. Crystal structure of DXO in complex with pAp-Mg^{2+}

To better understand the inhibitory mechanism of DXO by pAp, we determined the crystal structures of the wild-type and catalytic mutant (E234A) of mouse DXO in complexes with magnesium ion and pAp, at 1.8 Å and 1.9 Å resolution, respectively (Fig. 2). The complex was prepared by soaking the crystals of DXO free enzyme with a solution containing 100 mM pAp and 10 mM $MgCl_2$ for 90 min at 20°C. The pAp molecule was shown to be bound to a pocket composed of a-helices (αB, αC, αD, and αF), strand β12, and the aB-βó loop. Although the structures of the wild-type and E234A mutant are almost identical, the conformation of pAp was slightly different, especially with regard to the adenine ring (see Section 3.4 below). The determined structure showed good agreement with the X-ray diffraction data and the expected bond lengths, bond angles, and other geometric parameters (Table 1).

3.4. The pAp-bindingpocket

The electron density of pAp was clearly observed for the two phosphates and ribose, whereas the adenine ring showed a weaker electron density of the C2, N3, and C8 positions (Fig. 3A). The two magnesium ions have distinct electron densities, as previously observed for the DXO-pU5-Mg^{2+} complex structure [10]. The active site pocket fit well to accommodate the pAp molecule, and basic residues surround the two phosphates and ribose (Fig. 3B). While both of the phosphates of pAp are involved in the interaction with DXO, the 5’-end phosphate has extensive interactions with the residues Gln280, Glu192, and Lys255, as well as with the two magnesium ions (Fig. 3C). The 3’-end phosphate has a relatively weaker and direct interaction with Thr256, and shows an additional water-mediated interaction with the main chain of Gly188. The two magnesium ions are satisfied with an octahedral coordination sphere, and both metal ions are well overlaid with those of the product complex structure [10, 30]. In addition, as shown for the DXO-pU5 complex, the carbonyl oxygen of the Met185 residue, which is involved in discriminating RNA from DNA, interacts with the 2’-OH of the ribose ring. The Tyr189 residue has a base-stacking interaction with the adenine ring. Comparison of pAp with the wild-type and E234A mutant did not show any major conformational change; however, the adenine ring of pAp in the E234A mutant was more extended and rotated approximately 30 degrees outwards (Fig 3D). This result indicates that Glu234 is not involved in pAp recognition, and the position of Mg1 is not affected by the mutation of Glu234. In addition, since DXO has no sequence specificity, the conformation of the adenine ring in the pAp molecule could be slightly moved because it is not stabilized by residues at the active site.

3.5. Conformational comparison of pAp with other ligand-bound structures

To date, the apo- and five different ligands-bound structures of mouse DXO have been reported: apo and GDP [23], Cap analogue (m7GpppG), product pU5 (5’-end monophosphate penta-uracil nucleotides), and the substrate mimic pU(S)6 (5’-end monophosphate hexa-uracil nucleotides including phosphorothioate bonds at the 2nd and 3rd

positions) [10] and 3'-NADP$^+$ [15]. To investigate the binding mode of pAp, the structure of the DXO-pAp complex was superimposed to that of the DXO-pU5 complex. Interestingly, the pAp molecule overlapped well with the first nucleotide (U_2) of pU5, especially both the 5'- and 3'-end phosphates (Fig. 4A). Moreover, in comparison with pU(S)6, in contrast to pU5, the 5'-end phosphate was not overlaid and the 3'-end phosphate was also not perfectly matched, while the ribose and the bases were overlaid (Fig. 4B). This observation may reflect the fact that the conformation of pU(S)6 is not a real substrate but is considered a substrate mimic [10]. In addition, the position of Ca^{2+} and Mg1 differed. Although no correlated conformation was found in the superposed structures of pAp over m7GpppG, GDP, and 3'- NADP$^+$, none of these ligands could be accommodated in the active site together with pAp (Fig. 4C-E).

4. Discussion

Decapping by Dcp1/2 in conjunction with 5'−3' exoribonuclease Xrn1 activity is a well-known process of mRNA decay in eukaryotic cells [5]. In contrast, our previous studies suggested that DXO has activities of both decapping and 5'−3' exoribonuclease for quality control of mRNA during synthesis in yeast and mammals [10, 12]. Despite their similar ultimate effects, the catalytic mechanism and substrate specificity clearly differ between Dcp1/2 and DXO [31]. In addition, DXO and Xrn1 showed different substrate specificities and reactions [9, 12]. Besides Dcp1/2, some other mRNA decapping factors have been described, including scavenger decapping enzymes such as DcpS and Aph1/FHIT [32, 33], and Nudix hydrolase family members, including Nudt2, 3, 12, 15, 16, and 17 [34]. Moreover, Xrn1 is one of the best characterized 5'−3' exoribonucleases in eukaryotes. For example, recent studies suggest that Xrn1 could restrict hepatitis C virus replication [35], and downregulated autophagy-related transcripts under enriched fed conditions in yeast and mammalian cells [36]. Furthermore, in addition to its role in mRNA degradation, Xrn1 also interacts directly with decapping factors such as EDC4 and DCP1 in human and fruit fly cells mediated by the Dcp1 EVH1 domain and a Dcp1-binding motif in its C-terminal region [37].

In this study, we showed that pAp inhibited the nuclease activities of both DXO and Xrn1 *in vitro.* However, because DXO has relatively lower 5'−3' exoribonuclease activity than that of Xrn1, it was difficult to directly compare the inhibitory potency of pAp, which requires further verification *in vitro.* Both DXO and Xrn1 showed considerably weak pAp- binding affinity on the basis of their low Kd values of 20~30 mM range. This low binding affinity might explain why the pAp electron density could be obtained only in the presence of 100 mM pAp. Moreover, based on the crystal structure of the DXO-pAp complex, the pAp molecule is well overlapped on the second base of the substrate mimic ligand pU(S)6 as well as on the first base of the product pU5 that is in the vicinity of two magnesium ions. Therefore, pAp likely competes with the substrate RNA for binding to the active site. However, additional *in vitro* experiments may be needed to confirm the extent to which pAp interferes with the substrate RNA, such as a competition assays. Finally, as a step toward functional exploration of the interactions of DXO with pAp, it would also be interesting to investigate whether DXO is involved in intracellular Li^+ or Na^+-mediated toxicity as shown for Xrn1 [19].

Supplementary Material

Refer to Web version on PubMed Central for supplementary material.

Acknowledgements

We thank Ume Kalsoom Afridi for helpful discussion.

Funding

This work was supported by the Basic Science Research Program through the National Research Foundation of Korea (NRF) funded by the Ministry of Education, Science and Technology to JHC (2013R1A1A1061391 and 2016R1C1B2009691), a USA National Institutes of Health grant to LT (GM118093) and Medical University of South Carolina and Hollings Cancer Center to JHY.

Abbreviations:

DXO	decapping and exoribonuclease protein
NAD^+	nicotinamide dinucleotide
NMN	nicotinamide mononucleotide
m7GDP	7-methylguanosine diphosphate
pAp	3’, 5’-bisphosphate
pApS	3’-phosphoadenosine 5’-phosphosulfate

References

[1]. Moraes KC, RNA surveillance: molecular approaches in transcript quality control and their implications in clinical diseases, Mol Med, 16 (2010) 53–68. [PubMed: 19829759]

[2]. Orphanides G, Reinberg D, A unified theory of gene expression, Cell, 108 (2002) 439–451. [PubMed: 11909516]

[3]. Stutz F, Izaurralde E, The interplay of nuclear mRNP assembly, mRNA surveillance and export, Trends Cell Biol, 13 (2003) 319–327. [PubMed: 12791298]

[4]. Coller J, Parker R, Eukaryotic mRNA decapping, Annu Rev Biochem, 73 (2004) 861–890. [PubMed: 15189161]

[5]. Chang JH, Xiang S, Tong L, 5’−3’ exoribonucleases, in: Nicholson AW (Ed.) Ribonucleases, Springer-Verlag, Berlin, 2011, pp. 167–192.

[6]. Chen CY, Shyu AB, Mechanisms of deadenylation-dependent decay, Wiley Interdiscip Rev RNA, 2 (2011) 167–183. [PubMed: 21957004]

[7]. Chang JH, Xiang S, Tong L, Structures of 5’−3’ Exoribonucleases, Enzymes, 31 (2012) 115–129. [PubMed: 27166443]

[8]. Matos RG, Pobre V, Reis FP, Malecki M, Andrade JM, Arraiano CM, Structure and Degradation Mechanisms of 3’ to 5’ Exoribonucleases, in: Nicholson AW (Ed.) Ribonucleases, Springer-Verlag, Berlin, 2011, pp. 193–222.

[9]. Chang JH, Tong L, Substrate recognition and catalytic mechanism of 5’−3’ exoribonucleases, Biodesign, 2 (2014) 39–46.

[10]. Jiao X, Chang JH, Kilic T, Tong L, Kiledjian M, A mammalian pre-mRNA 5’ end capping quality control mechanism and an unexpected link of capping to pre-mRNA processing, Mol Cell, 50 (2013) 104–115. [PubMed: 23523372]

[11]. Jiao X, Xiang S, Oh C, Martin CE, Tong L, Kiledjian M, Identification of a quality- control mechanism for mRNA 5’-end capping, Nature, 467 (2010) 608–611. [PubMed: 20802481]

[12]. Chang JH, Jiao X, Chiba K, Oh C, Martin CE, Kiledjian M, Tong L, Dxo1 is a new type of eukaryotic enzyme with both decapping and 5’−3’ exoribonuclease activity, Nat Struct Mol Biol, 19 (2012) 1011–1017. [PubMed: 22961381]

[13]. Xue Y, Bai X, Lee I, Kallstrom G, Ho J, Brown J, Stevens A, Johnson AW, Saccharomyces cerevisiae RAI1 (YGL246c) is homologous to human DOM3Z and encodes a protein that binds the nuclear exoribonuclease Rat1p, Mol Cell Biol, 20 (2000) 4006–4015. [PubMed: 10805743]

[14]. Wang VY, Jiao X, Kiledjian M, Tong L, Structural and biochemical studies of the distinct activity profiles of Rai1 enzymes, Nucleic Acids Res, 43 (2015) 6596–6606. [PubMed: 26101253]

[15]. Jiao X, Doamekpor SK, Bird JG, Nickels BE, Tong L, Hart RP, Kiledjian M, 5’ End Nicotinamide Adenine Dinucleotide Cap in Human Cells Promotes RNA Decay through DXO-Mediated deNADding, Cell, 168 (2017) 1015-1027 e1010. [PubMed: 28283058]

[16]. Kiledjian M, Eukaryotic RNA 5’-End NAD(+) Capping and DeNADding, Trends Cell Biol, 28 (2018) 454–464. [PubMed: 29544676]

[17]. Cahova H, Winz ML, Hofer K, Nubel G, Jaschke A, NAD captureSeq indicates NAD as a bacterial cap for a subset of regulatory RNAs, Nature, 519 (2015) 374–377. [PubMed: 25533955]

[18]. Chen YG, Kowtoniuk WE, Agarwal I, Shen Y, Liu DR, LC/MS analysis of cellular RNA reveals NAD-linked RNA, Nat Chem Biol, 5 (2009) 879–881. [PubMed: 19820715]

[19]. Dichtl B, Stevens A, Tollervey D, Lithium toxicity in yeast is due to the inhibition of RNA processing enzymes, EMBO J, 16 (1997) 7184–7195. [PubMed: 9384595]

[20]. Thomas D, Surdin-Kerjan Y, Metabolism of sulfur amino acids in Saccharomyces cerevisiae, Microbiol Mol Biol Rev, 61 (1997) 503–532. [PubMed: 9409150]

[21]. Mechold U, Ogryzko V, Ngo S, Danchin A, Oligoribonuclease is a common downstream target of lithium-induced pAp accumulation in Escherichia coli and human cells, Nucleic Acids Res, 34 (2006) 2364–2373. [PubMed: 16682444]

[22]. Reinholt SJ, Ozer A, Lis JT, Craighead HG, Highly Multiplexed RNA Aptamer Selection using a Microplate-based Microcolumn Device, Sci Rep, 6 (2016) 29771. [PubMed: 27432610]

[23]. Xiang S, Cooper-Morgan A, Jiao X, Kiledjian M, Manley JL, Tong L, Structure and function of the 5’-->3’ exoribonuclease Rat1 and its activating partner Rai1, Nature, 458 (2009) 784–788. [PubMed: 19194460]

[24]. Otwinowski Z, Minor W, Processing of X-ray diffraction data collected in oscillation mode, Method Enzymol., 276 (1997) 307–326.

[25]. Brunger AT, Adams PD, Clore GM, DeLano WL, Gros P, Grosse-Kunstleve RW, Jiang JS, Kuszewski J, Nilges M, Pannu NS, Read RJ, Rice LM, Simonson T, Warren GL, Crystallography & NMR system: A new software suite for macromolecular structure determination, Acta crystallographica. Section D, Biological crystallography, 54 (1998) 905–921. [PubMed: 9757107]

[26]. Emsley P, Cowtan K, Coot: model-building tools for molecular graphics, Acta crystallographica. Section D, Biological crystallography, 60 (2004) 2126–2132. [PubMed: 15572765]

[27]. Sinturel F, Pellegrini O, Xiang S, Tong L, Condon C, Benard L, Real-time fluorescence detection of exoribonucleases, Rna, 15 (2009) 2057–2062. [PubMed: 19767421]

[28]. Drescher DG, Ramakrishnan NA, Drescher MJ, Surface plasmon resonance (SPR) analysis of binding interactions of proteins in inner-ear sensory epithelia, Methods Mol Biol, 493 (2009) 323–343. [PubMed: 18839357]

[29]. Barbas A, Matos RG, Amblar M, Lopez-Vinas E, Gomez-Puertas P, Arraiano CM, Determination of key residues for catalysis and RNA cleavage specificity: one mutation turns RNase II into a “SUPER-ENZYME”, The Journal of biological chemistry, 284 (2009) 20486–20498. [PubMed: 19458082]

[30]. Yang W, Nucleases: diversity of structure, function and mechanism, Q Rev Biophys, 44 (2011) 1–93. [PubMed: 20854710]

[31]. Jurado AR, Tan D, Jiao X, Kiledjian M, Tong L, Structure and function of pre- mRNA 5’-end capping quality control and 3’-end processing, Biochemistry, 53 (2014) 1882–1898. [PubMed: 24617759]

[32]. Liu H, Rodgers ND, Jiao X, Kiledjian M, The scavenger mRNA decapping enzyme DcpS is a member of the HIT family of pyrophosphatases, EMBO J, 21 (2002) 4699–4708. [PubMed: 12198172]

[33]. Taverniti V, Seraphin B, Elimination of cap structures generated by mRNA decay involves the new scavenger mRNA decapping enzyme Aph1/FHIT together with DcpS, Nucleic Acids Res, 43 (2015) 482–492. [PubMed: 25432955]

[34]. Grudzien-Nogalska E, Kiledjian M, New insights into decapping enzymes and selective mRNA decay, Wiley Interdiscip Rev RNA, 8 (2017).

[35]. Li Y, Yamane D, Lemon SM, Dissecting the roles of the 5' exoribonucleases Xrn1 and Xrn2 in restricting hepatitis C virus replication, J Virol, 89 (2015) 4857–4865. [PubMed: 25673723]

[36]. Delorme-Axford E, Abernathy E, Lennemann NJ, Bernard A, Ariosa A, Coyne CB, Kirkegaard K, Klionsky DJ, The exoribonuclease Xrn1 is a post-transcriptional negative regulator of autophagy, Autophagy, 14 (2018) 898–912 [PubMed: 29465287]

[37]. Braun JE, Truffault V, Boland A, Huntzinger E, Chang CT, Hass G, Weichenrieder O, Coles M, Izaurralde E, A direct interaction between DCPI abnd XRN1 couples mRNA decappingto 5' exonucleolytic degradation, Nat Struct Mol Biol, 19 (2012) 1324–1331. [PubMed: 23142987]

Highlights

- pAp inhibits the exoribonuclease activity of DXO
- Crystal structure of DXO was obtained in complex with pAp and Mg2+ at 1.8 Λ resolution
- pAp competitively inhibits DXO nuclease activity by sharing the binding site pocket

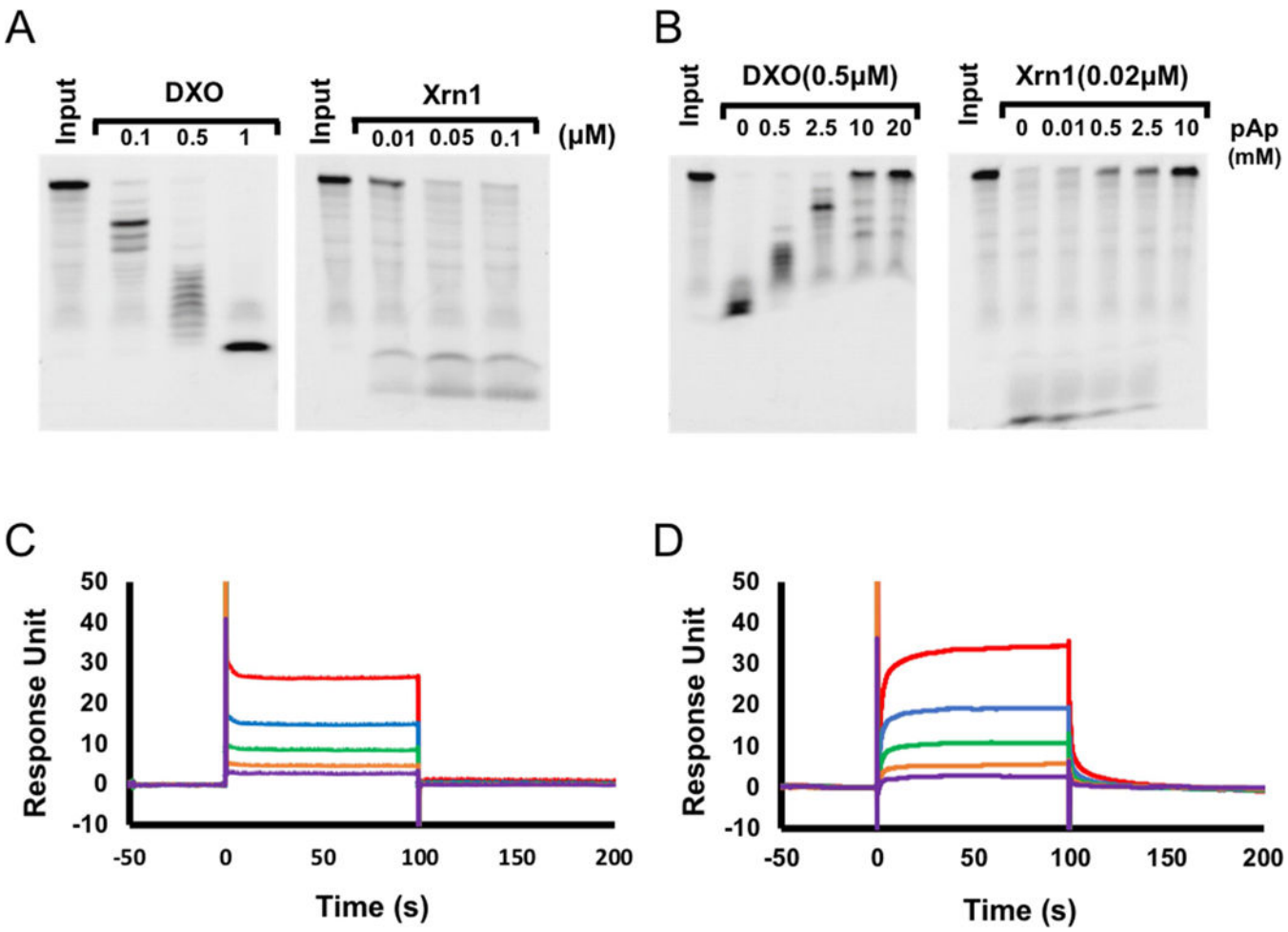

Figure 1. Inhibition of the 5'−3' exoribonuclease activity of DXO by pAp.

(A) Comparison of 5'−3' exoribonuclease activity between DXO and Xrnl. (B) Concentration- dependent inhibition of the 5'−3' exoribonuclease activity of DXO and Xrn1 by pAp. (C) Surface plasmon resonance experiment of DXO. A range of concentrations (0.5 ~ 8 mM) of pAp were injected to the DXO-immobilized cell. The colored lines indicate the concentration of pAp as following; Red, 8 mM; blue, 4 mM; green, 2 mM; orange, 1 mM; violet, 0.5 mM. (D) Surface plasmon resonance experiment of Xrn1. 0.5 ~ 8 mM of pAp were injected to Xrn1-immobilized cell (red, 8 mM; blue, 4 mM; green, 2 mM; orange, 1 mM; violet, 0.5 mM).

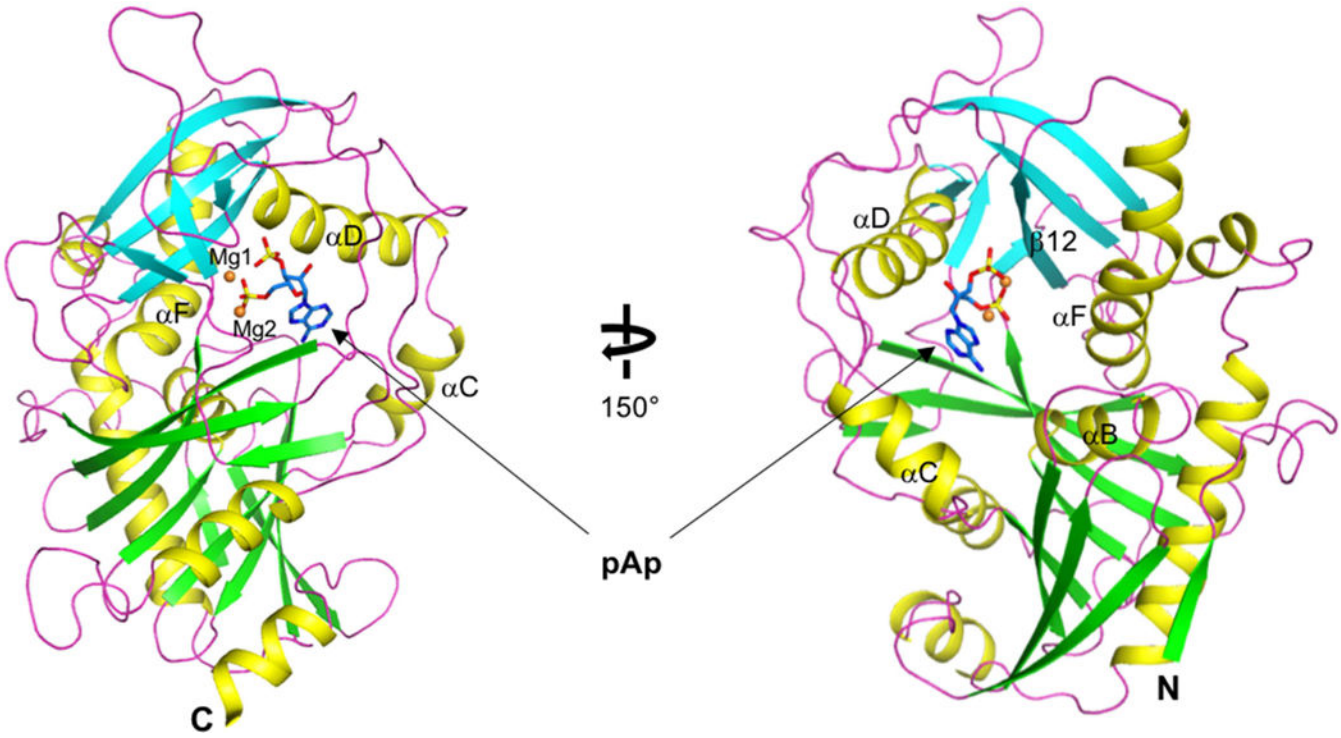

Figure 2. Overall structure of the DXO-pAp-Mg^{2+} complex.

Crystal structure of mouse DXO in complex with pAp-Mg^{2+} at 1.8 A resolution. The pAp molecule (light blue) is bound in the active site pocket. The right panel shows a different view (150° clockwise rotation) of the three-dimensional structure.

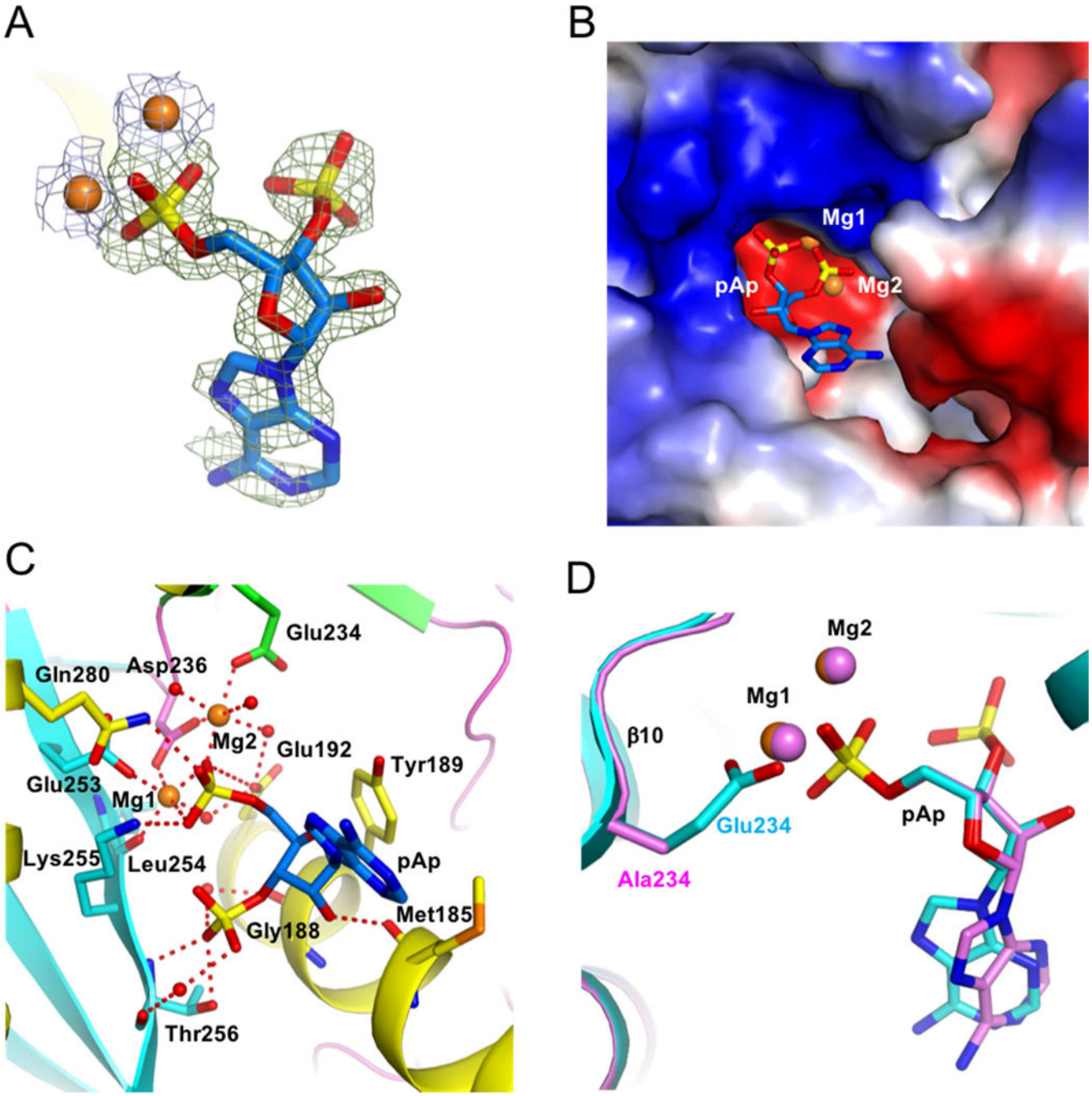

Figure 3. The pAp-binding pocket.

(A) Interactions between pAp with the active site. The 5'-phosphate interacts extensively with active-site residues via either magnesium ions or water molecules. The 3'-phosphate interacts with Thr256 and Gly188. Both magnesium ions (orange) are located in an octahedral coordination sphere. (B) Simulated-annealing omit 2Fo- Fc electron density at 1.8 A resolution for pAp, contoured at 1.0 σ. (C) The molecular surface of the active site pocket of DXO. The pAp molecule is bound with the two magnesium ions. (D) Conformational difference of the pAp molecules bound to the DXO wild-type (cyan) and

E234A mutant (violet). The two phosphates and ribose ring are almost identical but the position of the adenine ring is slightly different.

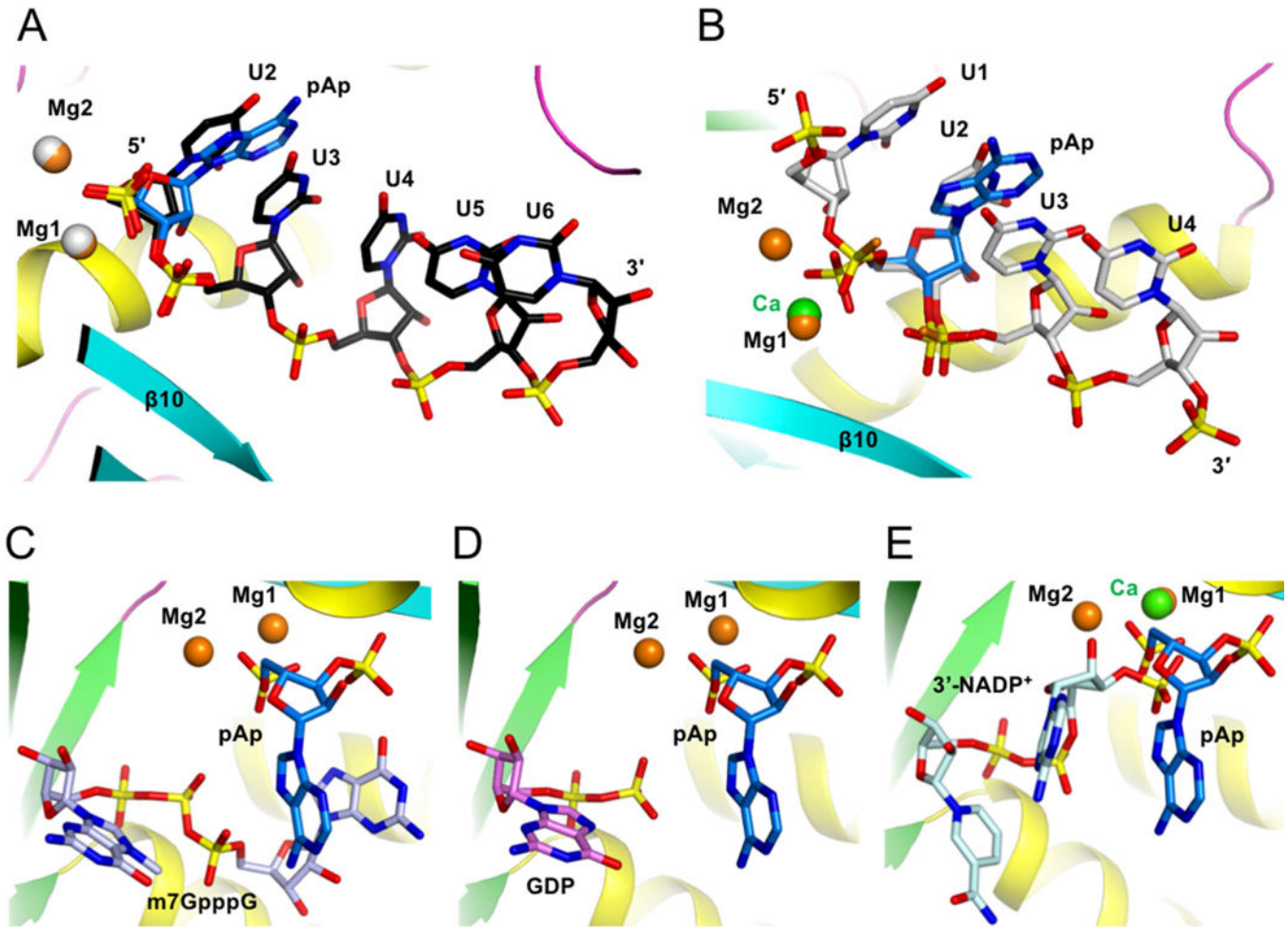

Figure 4. Conformational comparison of pAp with the RNA product, substrate mimic, and cap analogue.

(A) Overlay of the structures of DXO in complex with the RNA product (pU5)-Mg^{2+} and pAp-Mg^{2+}. The position of pAp (light blue) is well superposed with that of U2 in the RNA product (black). (B) Overlay of the structures of DXO in complex with the RNA substrate mimic-Ca^{2+} and pAp-Mg^{2+}. The position of pAp is well superposed with that of U2 in the RNA substrate mimic (white). (C) Overlay of the structures of DXO in complex with the Cap-analogue (m7GpppG, grey color) and pAp-Mg^{2+}. The two molecules are not superposed. (D) Overlay of the structure of DXO in complex with GDP (violet) and pAp-Mg^{2}+. (E) Overlay of the structure of DXO in complex with 3'-$NADP^{+}$ (light cyan) and pAp-Mg^{2+}.

Table 1.

Data collection and refinement statistics of the DXO-pAp-Mg2+ complex.

Statistics	Wild-type	E234A
Data collection		
Space group Cell dimensions (Å)	*P2i*	*P21*
a, b, c (Å)	46.46, 87.87, 50.10	46.50, 88.08, 50.04
α, β, γ (°)	90, 114.31, 90	90, 114.42, 120
Resolution (Å)	50.0 – 1.9 (1.86 – 1.80)	50.0 – 1.9 (1.97 – 1.90)
$^{R}merge^{b}$ (%)	5.7 (30.1)	6.0 (38.4)
I/σ (I)	21.7 (4.7)	21.7 (4.2)
Completeness (%)	98.9 (98.2)	99.0 (98.2)
Redundancy	3.7 (3.7)	3.8 (3.8)
Structure refinement		
Resolution (Å)	40.5 – 1.8 (1.84 – 1.80)	40.5 – 1.9 (1.95 – 1.90)
No. of reflections	33590 (2089)	28537 (1851)
$^{R}work$ / $^{R}free$	16.97 (20.37) / 19.92 (24 54)	17.02 (21.00) / 20.26 (29.03)
No. atoms		
Protein	2929	2893
Water	399	262
Ligand	29	29
R.m.s.deviation		
Bond lengths (Å)	0.006	0.006
Angles (°)	0.83	0.86
Average 5-factor (Å^2) Ramachandran plot (%)	28.8	30.3
Favored region	98.3	98.6
Outliers	0.0	0.0

[a] The numbers in parentheses are statistics from the highest resolution shell.

[b] $R_{merge} = \Sigma |I_{obs} - I_{avg}| / I_{obs}$, where I_{obs} is the observed intensity of individual reflection and I_{avg} is the average over symmetry equivalents.

[c] $R_{work} = \Sigma ||F_O| - |F_C|| / \Sigma |F_O|$, where $|F_O|$ and $|F_C|$ are the observed and calculated structure factor amplitudes, respectively. R_{free} was calculated with 5% of the data.